Dynamics of charge clouds ejected from laser-induced warm dense gold nanofilms

Jun Zhou, Alfredo A. Correa, Junjie Li, Shao Tang, Yuan Ping, Tadashi Ogitsu, Dong Li, Qiong Zhou, and Jianming Cao

Phys. Rev. E **90**, 041102 — Published 24 October 2014

DOI: 10.1103/PhysRevE.90.041102

Dynamics of charge clouds ejected from laser-induced warm dense gold nanofilms

Jun Zhou,[1] Alfredo A. Correa,[2] Junjie Li,[3] Shao Tang,[1] Yuan Ping,[2] Tadashi Ogitsu,[2] Dong Li,[1] Qiong Zhou,[1] and Jianming Cao[1]

[1]*Physics Department and National High Magnetic Field Laboratory, Florida State University, Tallahassee, Florida 32310, USA*
[2]*Lawrence Livermore National Laboratory, Livermore, California 94550, USA*
[3]*Brookhaven National Laboratory, Upton, New York 11973, USA*

We report the first systematic study of the ejected charge dynamics surrounding laser-produced 30-nm warm dense gold films using single-shot femtosecond electron shadow imaging and deflectometry. The results reveal a two-step dynamical process of the ejected electrons under the high pump fluence conditions: an initial emission and accumulation of a large amount of electrons near the pumped surface region followed by the formation of hemispherical clouds of electrons on both sides of the film, which are escaping into the vacuum at a nearly isotropic and constant velocity with an unusually high kinetic energy of more than 300 eV. We also developed a model of the escaping charge distribution that not only reproduces the main features of the observed charge expansion dynamics but also allows us to extract the number of ejected electrons remaining in the cloud.

PACS numbers:

Zapping target materials with intense, ultrashort laser pulses is the most widely used technique for producing high-energy density plasmas in the laboratory and facilitating applications such as laser micromachining [1], pulsed laser deposition [2, 3], plasma acceleration of relativistic high-energy charged particles [4], and inertial confinement fusion [5]. The intense laser-matter interaction associated with this method is quite intricate and involves an array of interesting physical processes including energy transport and exchange among subsystems, electron emission and recapture, charge separation, formation of transient magnetic fields, and implosion hydrodynamics. Disentangling this complex interaction relies on in-depth understanding of the deposition and redistribution of the laser energy in the targets as well as knowledge of the subsequent plasma dynamics. Most optical measurements of laser-induced plasma dynamics have been conducted using time-of-flight mass spectroscopy [6], time-resolved optical microscopy [7], optical emission spectroscopy [8, 9], and shadowgraphs [10]. These techniques have provided important insights into the processes of plasma formation and evolution but fall short of directly detecting the transient electric fields and the associated charge distribution and expansion dynamics.

Ultrafast electron shadow imaging and deflectometry [11–14] have recently emerged as new tools for probing charge and plasma dynamics via direct sensing of the correlated transient electric fields in real time. Warm dense matter (WDM) [15–17] has been the focus of these investigations because it is both central to understanding the convergence between condensed matter and plasma physics and relevant to broad research areas including shock physics [18], inertial confinement fusion [5], and planetary physics [19]. These studies have revealed that under the intense pump conditions of the widely used idealized slab plasma approach to create single-state WDM [20, 21] in the laboratory, significant numbers of hot electrons can be ejected from WDM targets by thermionic emission (TE), multiphoton photoemission (MPPE), or thermally assisted MPPE [22–26]. This ejection may break the charge neutrality and reduce the excitation energy density in the targets [27], thus altering subsequent formation and characteristics of WDM [15, 28]. To address these important issues, we conducted the first systematic measurement of the ejected charge cloud dynamics in the vicinity of a warm dense (WD) gold nanofilm using ultrafast electron shadow imaging and deflectometry in a single-shot mode. Based on these measurements, we developed a model for formulating the three-dimensional charge distributions of the ejected electrons, which allows us not only to reproduce the major features of the observed charge expansion dynamics but also to extract the number of ejected electrons.

The experimental setup of ultrafast electron shadow

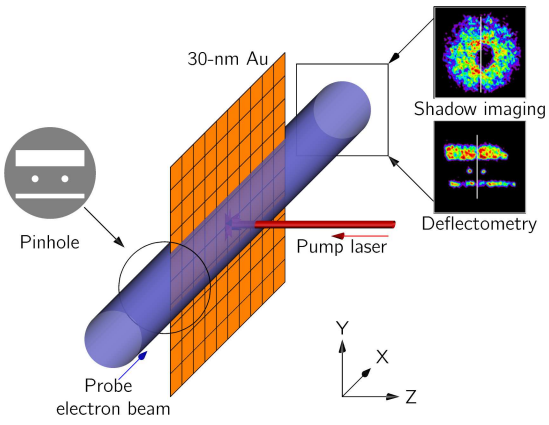

FIG. 1: (Color online) Schematic of ultrafast electron shadow imaging and electron deflectometry. The pump laser strikes the sample from the right side, and the vertical white line marks the original film position.

imaging and deflectometry was similar to that used in our previous work [11–13]. Fig. 1 shows the pump-probe geometry at the sample position. The sample is a 30-nm-thick freestanding gold film supported by a nickel mesh with a square mesh size of 386 μm. In the experiment, the WDM film was created by focusing 50-fs optical pulses on a 70-μm spot on the film surface, and the subsequent plasma dynamics were probed by passing 40-keV electron pulses across the plasma region. On average, each electron pulse contained roughly 2500 electrons and had a temporal duration of ~300 fs. For most of the measurements, the absorbed laser fluence was set at 3.0 J/cm^2, approximately 10 times higher than the ablation threshold of gold film. Therefore, the measurement had to be obtained in a single-shot mode, selecting a new sample position for each laser shot.

In the shadow image experiment, the electron beam transported freely with a relatively large beam diameter of 1.5 mm so that the overall feature of the transient electric field at both the front and the back sides could be tracked by recording and analyzing the distorted beam intensity profile (shadows). In the more quantitative deflectometry measurement, a specially designed metal disk containing two 50-μm pinholes positioned 400 or 600 μm apart was placed before the sample to create two confined electron beams passing parallel to the sample surface. By tracking the position changes of the deflected beam centers, we measured the transient electric field strength at a given passing distance-defined as impact parameter-from the film surface on both sides simultaneously.

Overall, the shadow images exhibited a temporal behavior similar to that observed previously with optically pumped metal slabs [11, 12]. After optical excitation, hemispherical shadows developed on both sides of the gold film and gradually increased in size by expanding further into the vacuum with time. The shadow radii showed a linear time dependence (see Fig. 2), indicating that the expansion rate of the charge cloud (shadow) is nearly isotropic and constant. After reaching 300 μm in approximately 20 ps, the front shadow edge gradually became blurry, with a concurrent fading of the shadows. Also, at a given time delay, the shadow size in front was larger than that in back.

Because shadow size correlates with the number of the ejected electrons, a larger shadow size in front of the film indicates a larger number of ejected electrons. Two mechanisms, MPPE and TE, contribute to this phenomenon [13]. In gold, MPPE requires at least four 800-nm photons to emit an electron at the Fermi level. Owing to this nonlinear relation, MPPE is much more pronounced in the front than in the back because of the short optical penetration depth: ~10 nm in gold at a wavelength of 800 nm. MPPE is nearly instantaneous and ceases after the laser pulse. By contrast, TE becomes significant after conduction electron reaches a high electron temperature (T_e) via electron thermalization. At the absorbed fluence of 3.0 J/cm^2, T_e is approximately 6.9 eV, estimated using temperature-dependent electronic specific heat [29, 30] and assuming that all the absorbed energy is retained in the electron subsystem. Therefore, electrons with energy above the vacuum level can escape from the WD gold film. This process usually lasts several picoseconds or longer until the T_e drops much lower than the vacuum level after electron-phonon thermalization and the electrons lose energy via TE. On the back, the number of TE electrons could be significantly less than that on the front if electron transport across the film has been somehow impeded [27, 28]. Overall, the intensity of MPPE is proportional to the fourth power of pump intensity, whereas that of TE depends linearly on the total absorbed energy.

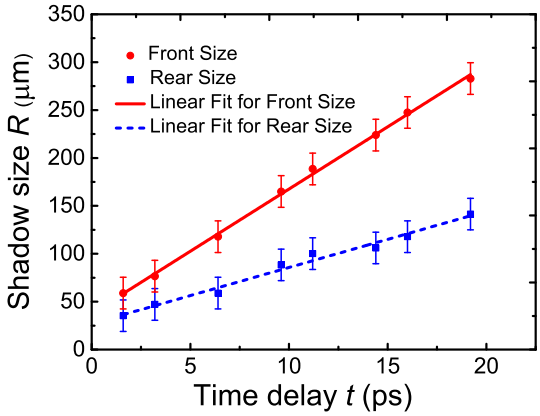

FIG. 2: (Color online) The radii of the hemispherical shadows at front and rear sides as a function of time delays. Solid red line and dashed blue line are linear fits with slope (1.3 ± 0.2) × 10^7 m/s and (5.8 ± 0.3) × 10^6 m/s for front and rear sizes, respectively.

Single-shot electron deflectometry measurements were also carried out to monitor the transient electric field in the vicinity of the laser-produced WD gold nanofilms. In the experiment, no apparent change in the beam profile was observed. Accordingly we used its center of mass to track the beam position. Fig. 3 shows the center of mass deflections as a function of time delays for both the front and the back with different impact parameters. In general, these beam deflection curves exhibit similar temporal behavior, rapidly approaching a positive maximum value followed by retracting and overshooting (negative deflection) to a negative maximum deflection before finally returning to the original position. The time to reach maximum deflection displays a linear dependence on the impact parameter, as shown in the insets in Fig. 3. By performing a linear fit, we extracted two effective rates-(1.2 ± 0.1) × 10^7 m/s in the front and (6.1 ± 0.3) × 10^6 m/s in the back-that are essentially the same as the speed of shadow edge motion obtained in the shadow imaging measurements (see Fig. 2). In reality, these two rates are correlated, because the probe beam is deflected backward toward the film once the front edge of the ejected charge cloud has passed beyond the probe beam. These rates

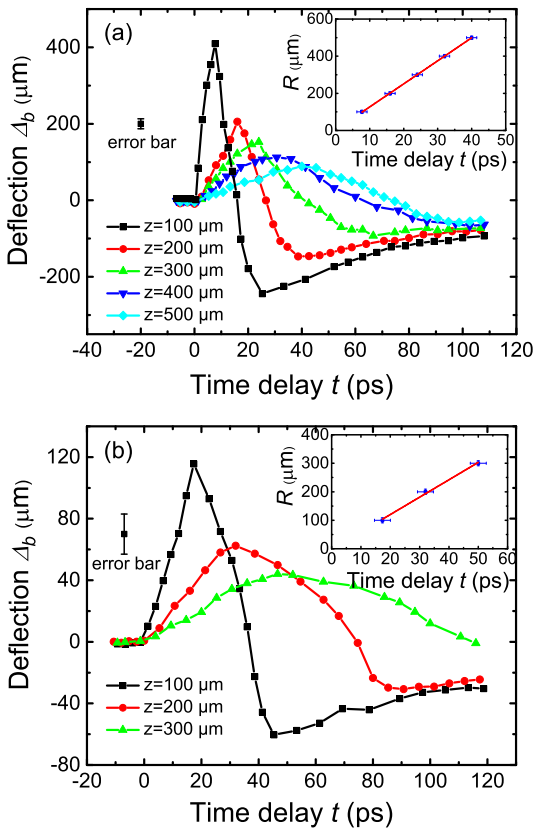

FIG. 3: (Color online) Deflection curves at different impact parameters at front (a) and at rear (b) sides of 30-nm gold film. The uncertainty of any given impact parameter is about 9 μm. Inset: charge cap size vs. time delay.

also agree well with those of a recent study [31] performed under similar experimental conditions.

Below we introduce a model of the ejected charge distributions to reproduce the results of the above shadow image and beam deflection measurements and calculate the number of electrons remaining in the escaping charge clouds. After intense optical excitation, a large number of electrons are ejected by MPPE and TE. Due to the space-charge (SC) effect [32–35], the ejected charge cloud undergoes self-expansion, pushing the electrons on the far side farther into the vacuum and the electrons closer to the film back to the film surface. The shadow image and beam deflection measurements have revealed a nearly hemispherical distribution of the ejected charges escaping at an isotropic and constant expansion rate. In addition, the probability of an electron escaping across the surface is dictated by the escape depth: $\Delta = \lambda\cos(\theta)$, where λ is the electron inelastic mean free path, and θ is the electron escape angle with respect to the surface normal [36]. Considering all the above conditions, we assumed that the escaping charge cloud also has a spherical shape with a density satisfying a $\cos(\theta)$ distribution. That is, the charge cloud could consist of a continuum of thin concentric hemispherical shells with a charge density expressed as follows:

$$\rho(r,\theta,t) = \frac{Q}{\pi R^2}\delta(r - R(t))\cos(\theta) \qquad (1)$$

where r is the distance to the shell center, θ is the polar angle, Q is the total charge on the sheet, and R is the shell radius at a given time delay t. Considering the relatively large shadow size (charge cloud size) of tens of microns as well as the short Debye length ($\lambda_D = 0.58$ Å) in gold, we can ignore the grainy nature of the gold film and treat its surface as an ideal grounded flat surface. Thus, at the front of the film, the shell charge distribution given by Eq. (1) together with its image charge generate an electric field that is dipolar outside the shell (pointing toward the surface) and uniform inside the shell (pointing away from the surface).

In the deflectometry measurement with an impact parameter b of 150 μm, the 40-keV electron beam traveled through the interaction region (approximately $2b$ [11]) in approximately 2 ps. During this period, the charge cloud expanded only approximately 20 μm-an expansion much smaller than the impact parameter. Thus, to the first approximation, we assumed that the charge cloud remains static, and the probe beam takes a snapshot of the transit electric field at a preset delay time. We can also neglect the contribution of the transient magnetic field to the beam deflection because of its negligible field strength for the current pumping intensity of 6×10^{13} W/cm^2 and the probe geometry used in our experiments [37, 38]. Under these conditions, the beam deflection at the detector due to one dipole sheet is given by the following:

$$\Delta_b = \begin{cases} \dfrac{eQL}{3\pi\varepsilon_0 K}\dfrac{R}{b^2}, & R < b \\ \dfrac{eQL}{3\pi\varepsilon_0 K}\dfrac{R^3 - \left(R^2+2b^2\right)\sqrt{R^2-b^2}}{R^2 b^2}, & R > b \end{cases} \qquad (2)$$

where L is the distance from the film to the detector, and K is the kinetic energy of the probe electrons. Given L and K, the deflection Δ_b is a function of $R(t)$, b and Q, with the timing implicitly contained in R.

This model reproduces the main features of electron shadow imaging and deflection measurements. It predicts that the deflection curves obtained at different impact parameters b can be rescaled to a universal curve, $\Delta_b \cdot b$ versus R/b, as long as the total charge Q, the beam energy K, and the camera length L remain unchanged. Fig. 4 shows the rescaled deflection curves acquired by normalizing the deflection data in Fig. 3 with their impact parameters. For both the front and the back (not shown in Fig. 4), all the normalized deflection curves fall into their own respective universal curves. The model prediction, generated by assuming the conservation of ejected charge Q, is plotted as a dashed blue line in Fig. 4.

To extract the amount of charge contained in the self-expanding charge cloud, we fit the universal scaled curve

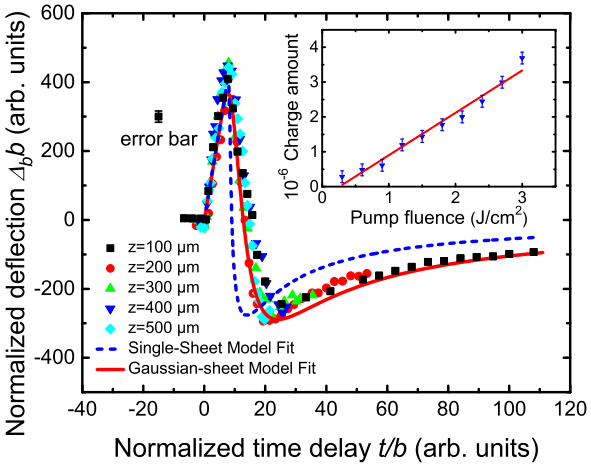

FIG. 4: (Color online) Rescaled front deflection curve. Inset: The amount of ejected charge at front surface as a function of absorbed fluences.

as a superposition of the deflections from a distribution of dipole sheets formulated above. In the fit, we assumed that the actual charge cloud contains a continuous distribution of dipole sheets. The weight of each sheet contribution to the beam deflection is regulated by its total charge, and the amount of charge on each sheet follows a Gaussian density profile along the radius that is centered at an effective R with a width of $2\sqrt{2\ln 2}\sigma$, where σ is one standard deviation and proportional to R. The fitting results, with $\sigma = (0.40 \pm 0.04)R$, an expansion velocity $\upsilon = (1.0 \pm 0.1) \times 10^7$ m/s and a total charge $Q_{tot} = (3.7 \pm 0.2) \times 10^6$ electrons per pulse, are plotted as a solid red line in Fig. 4. With this generalized model, agreement with the experimental results is quantitatively improved. Following the same protocol, we determined the ejected charge at the back to be $(9.1 \pm 0.2) \times 10^5$ electrons. We also measured the dependence of the deflection amplitude on the absorbed fluence, and the results are shown in the inset in Fig. 4. The amount of charge Q_{tot}, or the maximum defection, displays a clear linear dependence on the absorbed fluence, indicating that TE dominates the electron ejection process when the absorbed fluence is in the 0.3-3.0 J/cm^2 range used in this study.

The amount of effective charge extracted from our electron shadow imaging and deflection measurements using the above calculation is on the order of 10^6 electrons per shot (less than 1 electron per million atoms in the laser excited volume). This number is significantly smaller than the 10^{12} electrons predicted by the Richardson-Dushman equation, assuming no blockade of electron ejection [39]. We believe that the strong SC effect [32–35], which is concomitant with the electron emission process, is responsible for this discrepancy. The earliest emitted electrons tend to prevent the remaining hot electrons from being effectively ejected. In addition, the ejected charge cloud with high charge density undergoes self-expansion, pushing the electrons on the far side farther into the vacuum and the electrons closer to the film back to the film surface. Consequently, only a small portion of the entire ejected electrons are preserved in the escaping charge clouds. As proposed in other recent studies, the electron emission yield is reduced to below 1% even at a relatively low absorbed fluence of 1 mJ/cm^2 [35, 40], and further reduction is expected at a higher absorbed fluence [39]. Furthermore, many ejected electrons might remain right above the film surface and form a nanometer-thick electron sheath of high charge density [41]. This sheath would shield the electric field of the positively charged film left behind and reduce its influence on the passing probe electron beam. Owing to the combined effect of the electron sheath and the suppression of electron emission and escaping by the SC effect, only a very small portion of ejected electrons, showed up in our measurements. The energy removed by escaping electrons is estimated to be 2.5×10^{-10} J, much smaller than the absorbed energy of 1.5×10^{-4} J per pulse. Therefore, the escaping electrons alone should minimally reduce the excitation energy density of the WDM target.

An interesting observation revealed in this work is the ultrafast formation of hemispherical charge clouds that escape into the vacuum at a nearly isotropic and constant velocity of $\sim 1.0 \times 10^7$ m/s ($\sim$300 eV). Although the detailed creation dynamics remains to be resolved, we believe that the strong SC field induced by the emission of a large amount of low-energy electrons in an ultrashort picosecond or subpicosecond time scale again plays a crucial role. In addition to quenching the electron emission, the strong SC field accelerates the earlier ejected electrons to a high velocity on a time scale of a few picoseconds or shorter [40, 42]. The unusually high electron escaping kinetic energy of more than 300 eV indicates that the initial number of the ejected electrons (electron density) should be much higher than the electrons remained in the escaping charge clouds. All the above observations imply a two-step charge ejection dynamics under the high pump fluence conditions: an initial emission and accumulation of a large quantity of electrons near the pumped surface region followed by the formation of high energy charge clouds escaping into the vacuum at a nearly constant velocity. High-energy electrons of 30 eV produced by the SC effect were observed in a previous study of a femtosecond-laser-pumped gold single-crystal sample ($T_e = 1$ eV) [39]. Notably, once the ejected charge cloud reaches this stage of high kinetic energy, it preserves its high expanding velocity and shape in the subsequent expansion because the electric potential energy stored in the charge cloud is only about one-tenth that of the cloud kinetic-too small to alter the charge dynamics. The formation dynamics of this high-energy charge cloud in the initial stage of the laser-produced WDM nanofilms can provide a detailed knowledge of the two-step charge ejection dynamics revealed in this study and would be a compelling research topic for further investigations.

This work was supported by National High Magnetic

Field Laboratory and National Science Foundation Grant No. 1207252, and the High Energy Density Laboratory Plasmas (HEDLP) program of the U.S. Department of Energy. The work at Lawrence Livermore National Laboratory was performed under the auspices of the U.S. Department of Energy under contract No. DE-AC52-07NA27344.

[1] E.N. Glezer, M. Milosavljevic, L. Huang, R.J. Finlay, T.H. Her, J.P. Callan, and E. Mazur, Opt. Lett. **21**, 2023 (1996)
[2] C.T. Hebeisen, G. Sciaini, M. Harb, R. Ernstorfer, S.G. Kruglik, and R.J.D Miller, Phys. Rev. B **78**, 081403 (2008)
[3] P.R. M. Centurion, S. A. Trushin, F. Krausz and E. E. Fill, Nat. Photonics **2**, 315 (2008)
[4] Y.T. Li, X.H. Yuan, M.H. Xu, Z.Y. Zheng, Z.M. Sheng, M. Chen, Y.Y. Ma, W.X. Liang, Q.Z. Yu, Y. Zhang, et al., Phys. Rev. Lett. **96**, 165003 (2006)
[5] T.R. Dittrich, S.W. Haan, M.M. Marinak, S.M. Pollaine, D.E. Hinkel, D.H. Munro, C.P. Verdon, G.L. Strobel, R. McEachern, et al., Phys. Plasmas **6**, 2164 (1999)
[6] R. Stoian, D. Ashkenasi, A. Rosenfeld, and E.E.B. Campbell, Phys. Rev. B **62**, 13167 (2000)
[7] K. Sokolowski-Tinten, J. Bialkowski, A. Cavalleri, D. von der Linde, A. Oparin, J. Meyer-ter-Vehn, and S.I. Anisimov, Phys. Rev. Lett. **81**, 224 (1998)
[8] F. Claeyssens, M.N.R. Ashfold, E. Sofoulakis, C.G. Ristoscu, D. Anglos, and C. Fotakis, J. Appl. Phys. **91**, 6162 (2002)
[9] G. Zhang, D. Gu, X. Jiang, Q. Chen, and F. Gan, Appl. Phys. A **80**, 1039 (2005)
[10] T.Y. Choi, D.J. Hwang, and C.P. Grigoropoulos, Appl. Surf. Sci. **197198**, 720 (2002)
[11] J. Li, X. Wang, Z. Chen, R. Clinite, S.S. Mao, P. Zhu, Z. Sheng, et al., J. Appl. Phys. **107**, 083305 (2010)
[12] J. Li, X. Wang, Z. Chen, J. Zhou, S.S. Mao, and J. Cao, Appl. Phys. Lett. **98**, 011501 (2011)
[13] J. Li, J. Zhou, T. Ogitsu, Y. Ping, W.D. Ware, and J. Cao, High Energy Density Phys. **8**, 298 (2012)
[14] H. Park and J.M. Zuo, Appl. Phys. Lett. **94**, 251103 (2009)
[15] Y. Ping, D. Hanson, I. Koslow, T. Ogitsu, D. Prendergast, E. Schwegler, G. Collins, and A. Ng, Phys. Rev. Lett. **96**, 255003 (2006)
[16] R. Ernstorfer, M. Harb, C.T. Hebeisen, G. Sciaini, T. Dartigalongue, et al., Science, **323**, 1033 (2009)
[17] B.I. Cho, K. Engelhorn, A.A. Correa, T. Ogitsu, C.P. Weber, H.J. Lee, J. Feng, P.A. Ni, Y. Ping, A.J. Nelson, et al., Phys. Rev. Lett. **106**, 167601 (2011)
[18] A. Ng, T. Ao, F. Perrot, M.W.C. Dharma-Wardana, and M.E. Foord, Laser Part. Beams **23**, 527 (2005)
[19] D. Saumon, G. Chabrier, D.J. Wagner, and X. Xie, High Press. Res. **16**, 331 (2000)
[20] A. Ng, P. Celliers, A. Forsman, R.M. More, Y.T. Lee, F. Perrot, M.W.C. Dharma-wardana, and G.A. Rinker, Phys. Rev. Lett. **72**, 3351 (1994)
[21] A. Ng, A. Forsman, and P. Celliers, Phys. Rev. E **51**, 5208 (1995)
[22] S. I. Anisimov, B.L. Kapeliovich, T. L. Perel'man, Sov. Phys. JETP **39**, 375 (1974)
[23] G.P. Banfi, G. Ferrini, M. Peloi, and F. Parmigiani, Phys. Rev. B **67**, 035428 (2003)
[24] A. Apolonski, P. Dombi, G.G. Paulus, M. Kakehata, R. Holzwarth, T. Udem, C. Lemell, K. Torizuka, J. Burgdrfer, et al., Phys. Rev. Lett. **92**, 073902 (2004)
[25] G. Ferrini, C. Giannetti, G. Galimberti, S. Pagliara, D. Fausti, F. Banfi, and F. Parmigiani, Phys. Rev. Lett. **92**, 256802 (2004)
[26] F. Banfi, C. Giannetti, G. Ferrini, G. Galimberti, S. Pagliara, D. Fausti, and F. Parmigiani, Phys. Rev. Lett. **94**, 037601 (2005)
[27] T. Ogitsu, Y. Ping, A. Correa, B.-i. Cho, P. Heimann, E. Schwegler, J. Cao, and G.W. Collins, High Energy Density Phys. **8**, 303 (2012)
[28] Z. Chen, V. Sametoglu, Y.Y. Tsui, T. Ao, and A. Ng, Phys. Rev. Lett. **108**, 165001 (2012)
[29] Z. Lin, L.V. Zhigilei, and V. Celli, Phys. Rev. B **77**, 075133 (2008)
[30] http://www.faculty.virginia.edu/CompMat/electron-phonon-coupling/
[31] P. Zhu, Z. Zhang, L. Chen, J. Zheng, R. Li, W. Wang, J. Li, X. Wang, et al., Appl. Phys. Lett. **97**, 211501 (2010)
[32] N. H. Frank, Phys. Rev. **39**, 226 (1932)
[33] C. Girardeau-Montaut, J.P. Girardeau-Montaut, and H. Leboutet, Appl. Phys. Lett. **55**, 2556 (1989)
[34] C. Girardeau-Montaut and J.P. Girardeau-Montaut, Phys. Rev. A **44**, 1409 (1991)
[35] W. Wendelen, B.Y. Mueller, D. Autrique, B. Rethfeld, and A. Bogaerts, J. Appl. Phys. **111**, 113110 (2012)
[36] S. Hufner, Photoelectron spectroscopy (2003)
[37] C.K. Li, F.H. Sguin, J.A. Frenje, J.R. Rygg, R.D. Petrasso, R.P.J. Town, P.A. Amendt, S.P. Hatchett, O.L. Landen, et al., Phys. Rev. Lett **97**, 135003 (2006)
[38] T. Sokollik, M. Schnrer, S. Ter-Avetisyan, P.V. Nickles, E. Risse, M. Kalashnikov, W. Sandner, G. Priebe, M. Amin, et al., Appl. Phys. Lett. **92**, 091503 (2008)
[39] D.M. Riffe, X.Y. Wang, M.C. Downer, D.L. Fisher, T. Tajima, J.L. Erskine, and R.M. More, J. Opt. Soc. Am. B **10**, 1424 (1993)
[40] Z. Tao, H. Zhang, P.M. Duxbury, M. Berz, and C.-Y. Ruan, J. Appl. Phys. **111**, 044316 (2012)
[41] Y. Ping, A.A. Correa, T. Ogitsu, E. Draeger, E. Schwegler, T. Ao, K. Widmann, D.F. Price, E. Lee, H. Tam, et al., High Energy Density Phys. **6**, 246 (2010)
[42] X.Y. Wang, D.M. Riffe, Y.S. Lee, and M.C. Downer, Phys. Rev. B **50**, 8016 (1994)